Quantum confinement effects in semiconductor clusters. II

Antonietta Tomasulo and Mushti V. Ramakrishna
The Department of Chemistry, New York University, New York, New York 10003-6621

(Received 31 May 1995; accepted 14 May 1996)

The band gaps and spectral shifts of CdS, CdSe, CdTe, AlP, GaP, GaAs, and InP semiconductor clusters are calculated from band structure calculations using accurate local and nonlocal empirical pseudopotentials. The effect of spin-orbit coupling on the band structures is included in the calculations when they are important. The complete set of pseudopotential parameters and full computational details are reported for all these semiconductors. The calculated spectral shifts of zinc-blende and wurtzite CdS, wurtzite CdSe, zinc-blende CdTe, and zinc-blende InP clusters are in good agreement with experiments over a range of cluster sizes. The effect of crystal structure on the band gaps is small in large clusters but becomes important in small clusters. Spin-orbit coupling splits the valence band into *A*, *B*, and *C* sub-bands and we identify transitions arising from these sub-bands in the spectra of both CdSe and CdTe clusters. These results demonstrate that the empirical pseudopotential method yields unique insights into the quantum confinement effects and is a powerful quantitative tool for calculating the spectral shifts of semiconductor clusters. © *1996 American Institute of Physics.* [S0021-9606(96)01732-1]

I. INTRODUCTION

Clusters are an embryonic form of matter whose microscopic study provides insights into the evolution of material properties from molecules and surfaces to solids.[1–3] Furthermore, clusters have been shown to exhibit exotic optical properties and reactivities quite different from those in molecules and solids.[4–6] For these reasons, theoretical studies on clusters are critical to the design and synthesis of advanced materials with desired optical, electronic, and chemical properties.[7–16] Such studies are at the interface of the traditional fields of quantum chemistry, solid state chemistry, and statistical mechanics.[17–20] Hence, physicists, chemists, and material scientists are working individually and in teams to unearth the fundamental principles underlying the structure, dynamics, and reactivities of these clusters.[21–26] However, theoretical studies on the spectroscopy of semiconductor clusters have lagged far behind.[27]

The interest on the spectroscopy of semiconductor clusters arose from the discovery by Brus that such clusters can be synthesized in colloidal suspensions by controlled liquid phase precipitation reactions.[28] The radii of the clusters thus synthesized are usually in the 5-100 Å range. Furthermore, the x-ray and transmission electron microscopy (TEM) experiments have shown that these clusters have the same lattice structures as the corresponding bulk materials.[4,5,17,18,29] Finally, it is possible to prepare macroscopic samples of these clusters either in powder form or in colloidal suspension form. Such a versatility in sample preparation has made it possible for experimentalists to investigate the physical and optical properties of these clusters in detail.[4] Indeed, very sophisticated experiments are currently underway in various laboratories to understand the absorption spectra of these clusters as a function of the cluster size.[5,17–19] What is remarkable about these clusters is that their electronic spectra are not the same as that of the bulk, even though the clusters have the same structural properties as the crystals.[4] The absorption spectra of clusters show relatively sharp resonances superimposed on a continuum. The first absorption peak in the spectrum corresponds to the threshold for the absorption of light by the semiconductor cluster. It corresponds to the exciton energy, the energy needed to excite an electron from the top of the valence to the bottom of the conduction band. Quantitative prediction of the shift of the exciton energy with cluster size had been an outstanding problem for a decade. Simple theoretical calculations based on an effective mass model (EMM) were not successful and *ab initio* quantum chemistry electronic structure calculations are impossible for these clusters consisting of thousands of electrons. Consequently, what was needed was a model that captured the essential physics of the problem at hand.

Recently, we developed such a model.[30] We used accurate pseudopotentials to carry out band structure calculations and obtained the electronic energy levels of these clusters. Our calculations of the threshold for the absorption of light by CdS clusters yielded results in excellent agreement with experiment over a range of cluster sizes.[30] Furthermore, we predicted two new effects. First, we found that the exciton energies in small CdS clusters are sensitive to the crystal structure, even though such a sensitivity is absent in large clusters.[30] Second, we found that the vertical Franck-Condon transition energies in indirect gap clusters exhibit an anomalous redshift in small clusters.[30] In sharp contrast, the extant theoretical models always yielded monotonic blueshift of the transition energies with decreasing cluster size.[30]

The band structure model we employ here has also yielded a noteworthy insight into the nature of the electronic transitions in semiconductor clusters. The issue is whether the electronic transitions observed in these clusters are related in any way to the bulk transitions. Previous theoretical calculations implicitly assumed that the electronic states in semiconductor clusters are similar to those in molecules and hence they are qualitatively different from those in bulk.[31] In sharp contrast, our band structure model underlies the pre-

 0021-9606/96/105(9)/3612/15/$10.00

sumption that the electronic states in nanoscale clusters are similar to those in bulk. Consequently, we use the bulk language (direct vs indirect) to classify the electronic transitions in clusters. Recent experiments of Brus and co-workers[29] on the luminescence of Si clusters support our assumption. Based on the analysis of the luminescence of Si clusters, Brus and co-workers concluded that the lowest energy exciton transition is essentially an indirect gap transition, even though the spectrum has blueshifted by almost 0.9 eV.[29] This observation that mixing of k-states is weak in clusters supports our band structure model.

In this paper we extend our band structure calculations to a variety of other semiconductor clusters for three reasons: First, we wish to investigate the quantitative accuracy of our band structure model by repeating these calculations on different systems for which experimental data are now available. Second, the accuracy of our calculations on wurtzite clusters could not be verified previously because of the absence of experimental data on those clusters at that time. Third, we report the results of our investigation into the effect of spin-orbit coupling on the spectral transitions of CdSe and CdTe clusters. We also give the results of our calculations on AlP, GaP, GaAs, and InP clusters. While accurate and reliable experimental data on some of these clusters are not available at present, our calculations provide reasonable estimates of the expected spectral shifts as a function of cluster size.

Experimental synthesis of semiconductor clusters is still a challenging problem at present. One major difficulty is establishing a suitable synthetic route that yields nanometer scale clusters. The other major difficulty is determining optimal control parameters that yield clusters with a narrow size distribution. While both these problems remain to be fully solved, significant progress is being made daily. We hope the present paper will serve as a useful guide to the experimentalists on the expected behavior of spectral shifts in a variety of technologically important nanoscale semiconductor clusters.

This paper is organized as follows: in Section II we give the empirical pseudopotential theory of band structure calculations, in Sec. III we present the band structure model, in Sec. IV we give some computational details, and in Sec. V we present results of these calculations on a variety of semiconductor clusters. Finally, we summarize in Sec. VI.

II. EMPIRICAL PSEUDOPOTENTIAL METHOD

The electronic structure calculations of the semiconductor clusters are carried out using the empirical pseudopotential method (EMP).[30] This method consists of solving the Schrödinger equation using an empirically determined pseudopotential for the valence electron,

$$\mathscr{H} = -\frac{\hbar^2}{2m}\nabla^2 + V_p, \tag{1}$$

$$V_p(\mathbf{r},E) = V_L(\mathbf{r}) + \sum_{l=0}^{\infty} \Pi_l^{\dagger} A_l(E) f_l(\mathbf{r}) \Pi_l, \tag{2}$$

where the first term V_L is the purely local part, the second term gives the nonlocal (V_{NL}) part, and Π_l is the projection operator for angular momentum states l. The local part of the pseudopotential is given by

$$V_L(\mathbf{r}) = \sum_{\mathbf{G}} [V_S(\mathbf{G})S_S(\mathbf{G}) + iV_A(\mathbf{G})S_A(\mathbf{G})]\exp(i\mathbf{G}\cdot\mathbf{r}), \tag{3}$$

where V_S and V_A are the symmetric and anti-symmetric form factors, respectively, determined by fitting them to the experimental optical data. Similarly, S_S and S_A are the symmetric and anti-symmetric structure factors, respectively, determined from the crystal structure. The function $A_l(E)$ is the energy dependent well depth,

$$A_l(E) = \alpha_l + \beta_l[E^0(K)E^0(K')]^{1/2} - E^0(K_F)], \tag{4}$$

where $K=|\mathbf{G}+\mathbf{k}|$, $K'=|\mathbf{G}'+\mathbf{k}|$, $E^0(K)=\hbar^2K^2/2m$, and $K_F=(6\pi^2 z/\Omega_c)^{1/3}$ is the Fermi wave-vector with z the number of valence electrons per unit cell and Ω_c the volume of the unit cell. $f_l(\mathbf{r})$ is conveniently taken to be the square well,

$$f_l(\mathbf{r}) = \begin{cases} 1, & \mathbf{r} < R_l, \\ 0, & \mathbf{r} \geqslant R_l. \end{cases} \tag{5}$$

α_l, β_l, and R_l are the nonlocal parameters of the EPM theory to be determined from the experimental optical data on bulk crystals.

In many instances the local part of the pseudopotential (V_L) is sufficiently accurate to represent the gross features of the band structures correctly. However, the nonlocal pseudopotential is much more accurate over a broad range of energy scales.

The local contribution to the pseudopotential is given by Eq. (3). Evaluation of these matrix elements of the Hamiltonian for zinc-blende lattices is discussed in Ref. 30 and for wurtzite lattices in Appendix A. In the plane wave basis the matrix elements of the nonlocal pseudopotential are of the form[32]

$$V_{NL}(\mathbf{K},\mathbf{K}') = \frac{4\pi}{\Omega_a}\sum_{l,i} A_l^i(E)P_l(\cos(\Theta_{\mathbf{KK}'})) \times S^i(\mathbf{G}-\mathbf{G}')F_l^i(K,K'). \tag{6}$$

Spin-orbit coupling in band theory

In light elements the electron spin (s) and orbital angular momentum (l) are both good quantum numbers, since the magnetic field generated by the orbiting electron is too weak to induce coupling with the electron spin. However, in heavier elements the nearly relativistic speed of the electron produces a sufficiently large magnetic field that l and s are coupled, giving rise to $j=l+s$ as the good quantum number. The spin-orbit interaction thus couples electron dynamics in spin and ordinary spaces, thereby reducing the overall symmetry of the Hamiltonian. This relativistic effect is represented by the operator[33]

$$H_{SO} = \frac{\hbar}{4m^2c^2}\sigma\cdot(\nabla V_p \times p), \tag{7}$$

where σ are the Pauli spin matrices, V_p is the pseudopotential, p is the electron momentum, m is the true electron mass, and c is the speed of light. The matrix elements of H_{SO} in the plane wave representation are given by[34]

$$\langle \mathbf{K}',s'|H_{SO}|\mathbf{K},s\rangle = -i[\lambda_S S_S(\mathbf{G}-\mathbf{G}') + i\lambda_A \times S_A(\mathbf{G}-\mathbf{G}')](\mathbf{K}'\times\mathbf{K})\cdot\sigma_{ss'}. \quad (8)$$

For a binary semiconductor consisting of two types of atoms ($A \neq B$), we define

$$\lambda_S(K,K') = \tfrac{1}{2}(\lambda_1+\lambda_2), \quad \lambda_A(K,K') = \tfrac{1}{2}(\lambda_1-\lambda_2), \quad (9)$$

where

$$\lambda_1(K,K') = \mu B^A_{nl}(K)B^A_{nl}(K'),$$
$$\lambda_2(K,K') = \alpha\mu B^B_{nl}(K)B^B_{nl}(K'), \quad (10)$$

μ is the adjustable parameter chosen in order to obtain the splitting Δ of the valence band at Γ correctly. α is the ratio, Δ_A/Δ_B, of the spin-orbit splitting of the outermost p core orbital in isolated atoms A and B. Contributions from inner core or d-core states are neglected.[34] The atomic SO splitting values are taken from Herman-Skillman tables.[35] The momentum-space functions B_{nl} are defined as

$$B_{nl}(K) = C\int_0^\infty r^2 R_{nl}(r) j_l(Kr)\,dr, \quad (11)$$

where j_l are the spherical Bessel functions, C is determined by the condition

$$\lim_{K\to 0}\frac{B_{nl}(K)}{K^l} = 1, \quad (12)$$

and R_{nl} are the radial parts of the outermost electron wave functions taken from the Herman-Skillman tables.[35] We set $C=1$ in our calculations.

The band structures of semiconductors have several common features: In the zinc-blende structure the HOMO band is six-fold degenerate, counting the spin. The spin-orbit interaction splits this band into an upper four-fold degenerate Γ_8 component characterized by $(j,m_j)=(3/2,\pm 3/2)$ and $(3/2,\pm 1/2)$, and a lower two-fold degenerate Γ_7 component characterized by $(j,m_j)=(1/2,\pm 1/2)$.[36] The conduction band Γ_1 is two-fold degenerate.[37] In the wurtzite structure, the degeneracy of the valence band at Γ is removed by the crystal field, leading to an upper two-fold degenerate band and a lower four-fold degenerate band. The spin-orbit coupling further splits the lower band into two two-fold degenerate bands characterized by $(j,m_j)=(3/2,\pm 1/2)$ and $(1/2,\pm 1/2)$.[37] Both crystal field and spin-orbit interactions taken together thus give rise to three two-fold spin degenerate energy levels. In both structures, wurtzite and zinc-blende, these three valence bands are called heavy-mass $(3/2,\pm 3/2)$, light-mass $(3/2,\pm 1/2)$, and split-off $(1/2,\pm 1/2)$ band, respectively.[37] Transitions between these three valence bands to the conduction band are traditionally labelled A, B, and C.[38]

The atomic orbital approach is especially useful for describing valence bands near Γ. From this perspective, the HOMO bands arise from the valence p orbitals while the LUMO band arises from the s orbitals.[37] In polar semiconductors such as CdS and CdSe, HOMO bands originate primarily from the anion, and LUMO bands from the cation. However, in non-polar semiconductors such as CdTe and GaAs, considerable mixing of the cation and anion orbitals will take place.

III. BAND STRUCTURE MODEL

The virtue of EPM is that it reproduces the bulk band structures to better than 0.1 eV accuracy.[30,39] The calculations based on the density functional theory (DFT) typically underestimate the band gaps by about 30–50%. The DFT based methods optimize the orbitals of the occupied electronic states only, not those of the unoccupied orbitals. This problem remains even when nonlocal density gradient corrections and other higher-order improvements to the DFT methodology are made. Furthermore, the DFT calculations are computationally far more expensive compared to EPM. Similarly, the empirical tight-binding models, while being accurate in principle, are also compute intensive. Hence, EPM is appropriate for the investigation of the electronic structures of semiconductor clusters.

To apply EPM to the electronic structure calculations of the semiconductor clusters we assume that these clusters have the crystal structure of the bulk semiconductor. This assumption is justified because we are considering relatively large clusters containing tens to hundreds of atoms. The x-ray and TEM experiments on Si, CdS, CdSe, CdTe, GaAs, and InP clusters have shown that the bulk lattice structure is preserved even when the cluster radii are as small as $\mathbf{R}=7$ Å.[4,5,17–19,25] The reason for the preservation of the bulk lattice structure even in such small clusters is due to the presence of ligands on the surfaces of these clusters. The ligands are necessary to prevent the clusters from coalescing into larger units. These ligands also terminate the dangling bonds on the surfaces of these clusters, and thus inhibit structural reconstruction. For this reason, even small clusters seem to possess bulk lattice structure. The major effect of size on cluster structures seems to be small contractions of the bond lengths relative to their bulk values.

The band structure calculations are carried out for these clusters in almost the same way as we had done previously for CdS.[30] In bulk semiconductors the allowed wave-vectors $\mathbf{k}$ of the electronic states are continuous. On the other hand, only discrete $\mathbf{k}$-states are allowed in clusters. If we model the cluster as a rectangular box with dimensions L_x, L_y, and L_z, then a reasonable approximation is to use the bulk pseudopotential $V_p(\mathbf{r})$ inside the cluster and terminate this potential at the surfaces of the cluster by an infinite potential. The wave-vectors of the lowest allowed states are then given by the quantization condition $\sin(k_xL_x)\sin(k_yL_y)\sin(k_zL_z)=0$, whose solution is

$$\mathbf{k}=\pi\left(\frac{n_x}{L_x},\frac{n_y}{L_y},\frac{n_z}{L_z}\right), \tag{13}$$

where n_x, n_y, and n_z are the quantum numbers of a particle in a box with infinite potentials at the boundaries. The surface ligands act as potential barriers to the valence electrons. Consequently, for low energy excitations under consideration, the assumption of infinite potentials at the boundaries is a good approximation.

Similarly, if we model the cluster as a spherical object of radius R, the energy levels of the valence electrons will be quantized because of the spherical boundary. The wavevectors of the lowest allowed states are given by $j_0(k_nR)=0$, whose solution is $k_n=n\pi/R$.[40] Since k_n is along the radial direction, we project it onto each of the Cartesian axes with equal magnitude to obtain Cartesian components of **k**. This procedure yields

$$\mathbf{k}=\frac{\pi}{\sqrt{3}R}\,(n_x,n_y,n_z), \tag{14}$$

for spherical clusters. While **k** is not an exact quantum number in a finite cluster, it is a good first approximation in relatively large clusters, as discussed elsewhere.[30] Sometimes we also model spherical clusters as cubic boxes with $L=2R$ as the sidelength of the cube.[30] The energy levels at these allowed **k**-states constitute the band structure of a spherical cluster.

The exciton energy of a cluster of radius R is given by[4,41]

$$E_x=E_g-\frac{1.786}{\epsilon R}-0.248E_{Ry}, \tag{15}$$

where E_g is the HOMO–LUMO band gap, ϵ is the dielectric constant, $E_{Ry}=\mu e^4/2\epsilon^2\hbar^2$ is the effective Rydberg energy of the exciton, and μ is the reduced mass of the electron-hole pair. The second term in this equation, accounting for the Coulomb attraction between the electron-hole pair, is obtained by Brus through perturbation theory using effective mass wavefunctions.[4] The third term in the above equation is the correlation correction derived by Kayanuma.[41]

EPM has been shown to reproduce the band gaps to within 0.1 eV for both bulk materials and clusters.[30] Specifically, our predicted indirect band gap of 0.43 eV for a 10 Å radius silicon cluster was found to be in good agreement with recent experimental value of 0.5 eV obtained by Louis Brus and co-workers.[42] Likewise, EPM yielded excellent results for CdS clusters in comparison with experiment.[30] Full details on the computational methodology are given in Ref. 30.

IV. COMPUTATIONAL DETAILS

Table I lists the parameters of the pseudopotentials of zinc-blende and wurtzite CdS and CdSe clusters, while Tables II–IV list the corresponding parameters for the pseudopotentials of zinc-blende CdTe, AlP, GaP, GaAs, and InP clusters. Spin-orbit interaction was included in the calculations of wurtzite CdS, wurtzite CdSe, zinc-blende CdTe, and InP clusters. We have verified that the spin-orbit effects are small in AlP, GaP, and GaAs crystals. Consequently, our calculations on these clusters omitted the spin-orbit interaction in the Hamiltonian.

We used the radial Hartree–Fock–Slater orbitals $4p$ for cadmium, $5p$ for indium, $2p$ for sulphur, $3p$ for selenium, $4p$ for tellurium, and $2p$ for phosphorus in our calculations employing spin-orbit interaction in the Hamiltonian.

We use the standard notation to represent the high symmetry points in the Brillouin zone.

V. RESULTS AND DISCUSSION

A. CdS and CdSe clusters

The CdS and CdSe crystals exist in both zinc-blende and wurtzite forms, with the wurtzite form being the ground state structure. In principle it is possible to synthesize clusters also in both these lattice forms. However, the CdS clusters seem to prefer zinc-blende over wurtzite, while CdSe clusters seem to prefer wurtzite over zinc-blende structure. The possibility of being able to synthesize both these isomeric forms of CdS and CdSe clusters provides us an opportunity to investigate the effect of lattice structure on the exciton energies as a function of cluster size.

We use the lattice constant $a_0=5.82$ Å for zinc-blende and $a_0=4.14$ Å for wurtzite CdS crystals. Our calculated band gaps are 2.44 and 2.52 eV for bulk zinc-blende and wurtzite CdS, respectively. The experimental result is 2.50 eV[41] for both these structures.

We use the lattice constant $a_0=6.08$ Å for zinc-blende and $a_0=4.30$ Å for wurtzite CdSe crystals. The calculated band gaps are 1.92 and 1.79 eV for bulk zinc-blende and wurtzite CdSe, respectively. The experimental values for bulk wurtzite CdSe are 1.75 and 1.83 eV at 80 and 293 K, respectively. We take the average of these two values, 1.79 eV, as the experimental value for both zinc-blende and wurtzite CdSe crystals.

For both zinc-blende and wurtzite systems we have used the form factors empirically determined by Bergstresser and Cohen[43] and reported in Table I. For wurtzite structures the fundamental band gap without spin-orbit coupling ($\Gamma_6^v\rightarrow\Gamma_1^c$) is $E_a+1/3\Delta$, where E_a is the value of the band gap with spin-orbit coupling ($\Gamma_9^v\rightarrow\Gamma_7^c$) and Δ is the value of the spin-orbit splitting. The spin-orbit coupling parameter μ was chosen in order to satisfy this condition to better than 0.001 eV accuracy. For the CdS crystal, Δ is 0.07 eV[44] and we determined that $\mu=0.001$ is optimal. For the CdSe crystal, Δ is 0.43 eV[44] and we determined that $\mu=0.012$ is optimal.

Figure 1(a) shows the band structure of a zinc-blende CdS crystal and comparison with the experimental data,[45] while Fig. 1(b) shows the band structure of a wurtzite CdS crystal. The discrete energy levels of a $R=15.0$ Å wurtzite CdS cluster, modelled as a sphere of radius R, are given in Fig. 1(c). Figure 2(a) is the band structure of a zinc-blende CdSe crystal compared with the available experimental data[45] and Fig. 2(b) is the band structure of a wurtzite CdSe crystal.

TABLE I. Reciprocal lattice vectors and form factors (in a.u.) for CdS and CdSe crystals.

		CdS		CdSe	
G	G^2	$\mathbf{V}_S$	$\mathbf{V}_A$	$\mathbf{V}_S$	$\mathbf{V}_A$
Zinc-blende					
000	0	0.000	0.000	0.000	0.000
111	3	−0.120	0.115	−0.115	0.095
200	4	0.000	0.065	0.000	0.060
220	8	0.015	0.000	0.005	0.000
311	11	0.020	0.025	0.020	0.025
222	12	0.000	0.025	0.000	0.025
400	16	0.000	0.000	0.000	0.000
Wurtzite					
000	0	0.000	0.000	0.000	0.000
001	$\frac{3}{4}$	0.000	0.000	0.000	0.000
100	$2\frac{2}{3}$	−0.130	0.000	−0.125	0.000
002	3	−0.120	0.115	−0.115	0.095
101	$3\frac{3}{12}$	−0.100	0.090	−0.100	0.075
102	$5\frac{2}{3}$	−0.015	0.040	−0.035	0.045
003	$6\frac{3}{4}$	0.000	0.000	0.000	0.000
210	8	0.015	0.000	0.005	0.000
211	$8\frac{3}{4}$	0.000	0.000	0.000	0.000
103	$9\frac{5}{12}$	0.020	0.025	0.015	0.025
200	$10\frac{2}{3}$	0.020	0.000	0.020	0.000
212	11	0.020	0.025	0.020	0.025
201	$11\frac{5}{12}$	0.020	0.025	0.020	0.025
004	12	0.000	0.025	0.000	0.025
202	$13\frac{2}{3}$	0.010	0.015	0.010	0.015
104	$14\frac{2}{3}$	0.000	0.010	0.000	0.010
213	$14\frac{3}{4}$	0.000	0.000	0.000	0.000

The study of the dependence of the excitonic energies on the cluster size has been carried out using the bulk crystal parameters reported in Table V. Since for a CdS cluster of radius $R=100$ Å the fundamental gap is 2.46 eV for zinc-blende, and 2.55 eV for wurtzite, we shifted our conduction energy levels by $+0.04$ eV and -0.05 eV, respectively, in order to obtain the experimental bulk band gap of 2.50 eV. We carried out a similar correction for CdSe clusters, shifting the conduction bands by -0.15 eV for zinc-blende and -0.025 eV for wurtzite, so that we obtain the bulk band gap of 1.79 eV for a cluster of $R=100$ Å.

In Fig. 3 we compare the calculated exciton energies of both wurtzite and zinc-blende CdS clusters with the experimental data.[28,46–49] This figure clearly shows that the zinc-blende and wurtzite clusters exhibit different spectral shifts and the available experimental data follow one or the other of these trends. Based on these calculations, we can assign the zinc-blende structure to the clusters synthesized by Wang and Herron[48] and wurtzite structure to the smaller clusters synthesized by Weller and co-workers.[49]

In Figs. 4(a) and 4(b) we present the exciton energies of zinc-blende and wurtzite CdSe clusters calculated without spin-orbit coupling. The experimental data are superimposed on the calculated results for comparison.[25,50–59] Agreement between theory and experiment is only modest for zinc-blende clusters. This is primarily due to the broad size distribution of the clusters, which were mostly synthesized in glasses where size control is difficult to achieve. For this reason, the exciton energies of zinc-blende clusters do not follow any trend. On the other hand, high quality data exist

TABLE II. The nonlocal pseudopotential parameters of the semiconductors. The parameters V_S, V_A, α_0, and A_2 are in a.u., a_0 is in Å, and β_0, μ, and α are dimensionless. Observe that using only the local parameters of the pseudopotential given below does not yield correct band structures of the semiconductors.

Compound	$V_S(\sqrt{3})$	$V_S(\sqrt{8})$	$V_S(\sqrt{11})$	$V_A(\sqrt{3})$	$V_A(\sqrt{4})$	$V_A(\sqrt{11})$	a_0 (Å)	
Local parameters								
CdTe	−0.11000	0.00000	0.03100	0.03000	0.02500	0.01250	6.48	
AlP	−0.12250	0.01000	0.02000	0.05000	0.03000	0.00005	5.46	
GaP	−0.11500	0.01000	0.02850	0.05000	0.03500	0.01250	5.45	
GaAs	−0.10700	0.00700	0.03350	0.02750	0.01900	0.00050	5.65	
InP	−0.11750	0.00000	0.02650	0.04000	0.03000	0.01500	5.86	
Nonlocal parameters								
		Cation			Anion		Spin orbit	
	α_0	β_0	A_2	α_0	β_0	A_2	μ	α
CdS (wz)	⋯	⋯	⋯	⋯	⋯	⋯	0.0010	4.158
CdSe (wz)	⋯	⋯	⋯	⋯	⋯	⋯	0.0120	0.951
CdTe	0.000	0.400	0.000	0.000	0.400	1.000	0.0225	0.609
AlP	0.190	0.300	0.350	0.160	0.030	0.180	⋯	⋯
GaP	0.000	0.300	0.200	0.160	0.050	0.225	⋯	⋯
GaAs	0.000	0.000	0.063	0.000	0.000	0.313	⋯	⋯
InP	0.000	0.250	0.275	0.150	0.050	0.175	0.0095	1.000

on wurtzite CdSe clusters and our calculations displayed in Fig. 4(b) reproduce their overall trend fairly closely.

The exciton energies of wurtzite CdSe clusters, however, do exhibit considerable scatter, as seen in Fig. 4(b). To investigate the origin of this scatter, we considered the effect of spin-orbit coupling on the exciton energies. Since Se is a heavy element, spin-orbit coupling is much more important in CdSe than in CdS.

In a bulk wurtzite CdSe semiconductor, the degeneracy of the valence band at Γ is first removed by the crystal field, leading to an upper twofold spin degenerate band and a lower fourfold spin degenerate band. The spin-orbit coupling further splits the lower band into two twofold degenerate bands characterized by $(j,m_j)=(3/2,\pm 1/2)$ and $(1/2,\pm 1/2)$.[37] The combined influence of these crystal field and spin-orbit effects is to give rise to three distinct transitions, labelled A, B, and C. If we assume that similar transitions exist in clusters too, then we obtain the transitions shown in Fig. 4(c). Since the bulk transition A is at 1.79 eV,[44] and that for a cluster of $R=100$ Å is at 1.67 eV (using 233 plane waves), a correction of $+0.12$ eV was applied. The calculated transitions B and C were also similarly corrected: B bulk transition=1.81 eV,[44] cluster ($R=100$ Å) $=1.74$ eV, so the correction=0.07 eV; C bulk transition $=2.22$ eV,[44] cluster ($R=100$ Å)=2.16 eV, so the correction $=0.06$ eV. From Fig. 4(c) we observe that if only the lowest exciton energies are considered, then the experimental data show significant scatter compared to the calculated results. However, when we consider all three transitions (A, B, and C), then all the experimental data can be neatly accounted for as belonging to one of these three transitions. This finding indicates the possibility that some of the experimental data reported in the literature correspond to higher energy transitions (B and C) rather than to the lowest energy transition A.

Indeed, a more detailed comparison between our calculations and the available experimental spectral data due to the splitting of the valence band of wurtzite CdSe clusters[25,53,54,56–58] supports this assertion. The agreement between our calculated C transitions and the experimental split-off data of Bawendi and collaborators (open left triangle[25]), Peyghambarian and collaborators (open up triangle[57]), and Ekimov and collaborators (filled down triangles[58]) is very good. Based on these calculations we also re-assign the second quantum confined transitions E_2 reported by Borrelli and collaborators[56] and the second transition of the $R=16$ Å cluster sample reported by Woggon *et al.*[54] as belonging to C.

The spectroscopy of nanoscale CdS and CdSe clusters has attracted considerable attention from several research groups.[25,28,46–59] Some of these groups have succeeded in synthesizing cluster samples that have very narrow size distributions.[25,48,49,52,59] Furthermore, they have made very careful measurements of the exciton energies. For these rea-

TABLE III. The nonlocal pseudopotential parameters R_0 and R_2 in Å.

Compound	Cation		Anion	
	R_0	R_2	R_0	R_2
CdTe	1.37	1.41	1.06	1.41
AlP	1.06	1.19	1.06	1.19
GaP	1.27	1.19	1.06	1.19
GaAs	1.27	1.44	1.06	1.44
InP	1.27	1.29	1.06	1.29

TABLE IV. The pseudopotential parameters of GaP and GaAs semiconductors used in purely local EPM calculations. The parameters V_S and V_A are in a.u.

Compound	$V_S(\sqrt{3})$	$V_S(\sqrt{8})$	$V_S(\sqrt{11})$	$V_A(\sqrt{3})$	$V_A(\sqrt{4})$	$V_A(\sqrt{11})$
GaP	−0.11250	0.01200	0.03800	0.06400	0.02650	0.01000
GaAs	−0.12250	−0.00250	0.03750	0.03100	0.01750	0.00150

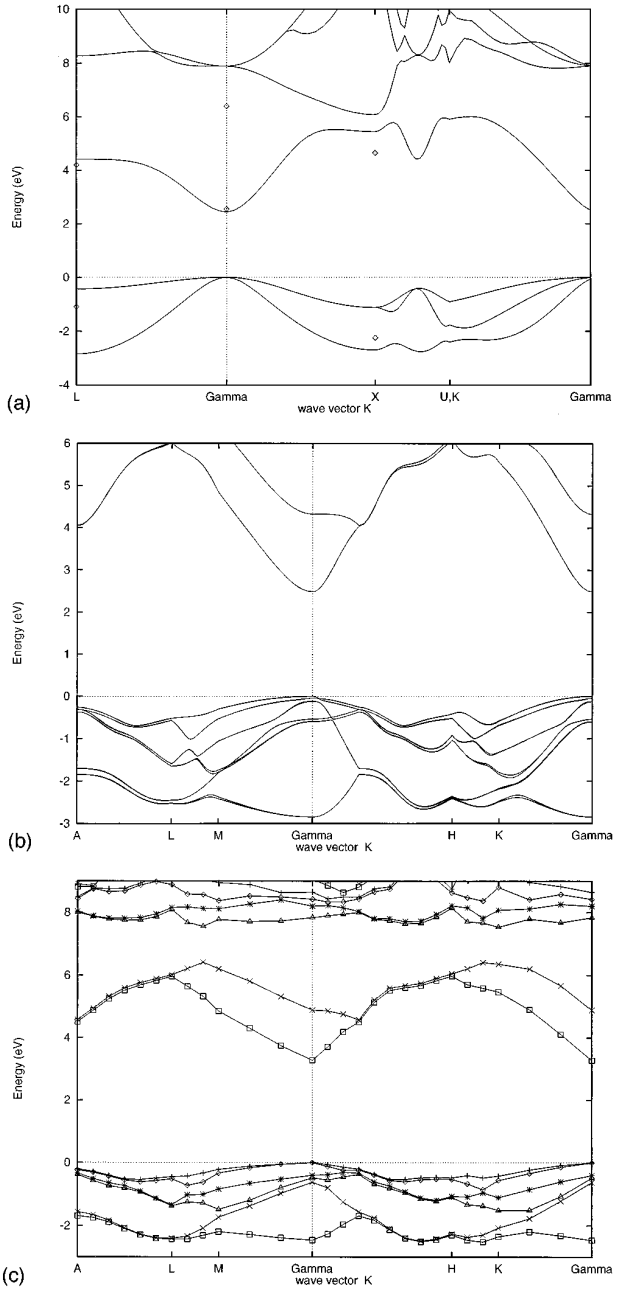

FIG. 1. (a) Band structure of a zinc-blende CdS crystal obtained using 283 plane waves. Experimental data are superimposed on the band structure for comparison.[45] (b) Band structure of a wurtzite CdS crystal obtained using 233 plane waves and with the inclusion of the spin-orbit interaction in the Hamiltonian. (c) Allowed electronic levels of a wurtzite CdS spherical cluster ($R=15$ Å) obtained using 233 plane waves.

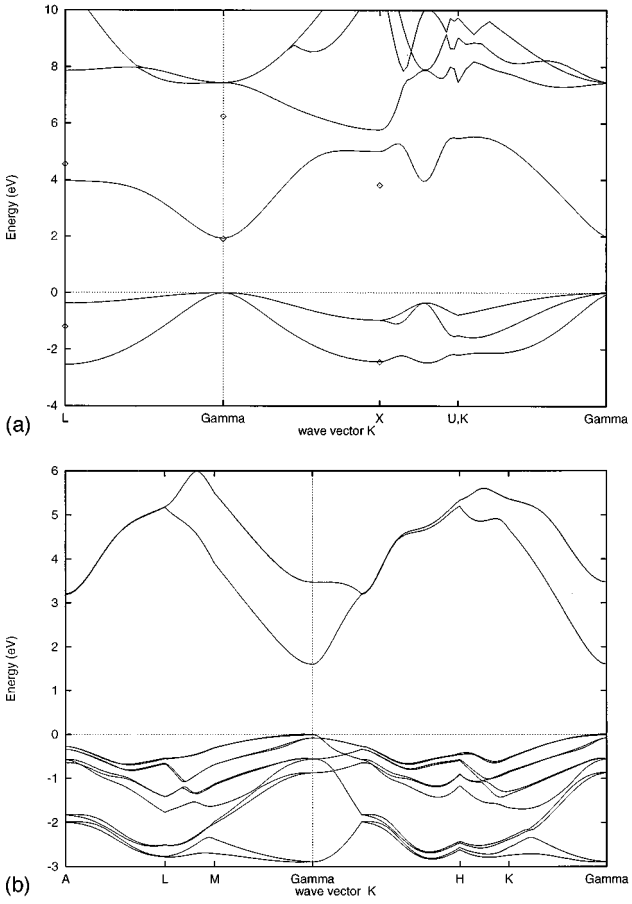

FIG. 2. (a) Band structure of a zinc-blende CdSe crystal obtained using 283 plane waves. Experimental data are superimposed on the band structure for comparison.[45] (b) Band structure of a wurtzite CdSe crystal obtained using 233 plane waves and with the inclusion of the spin-orbit interaction in the Hamiltonian.

sons, direct comparison between our calculations and the data from these groups provides a benchmark test of the reliability of our computational method in yielding accurate exciton energies. From the results presented in Figs. 3 and 4 it is clear that the agreement between our calculations and experimental data is excellent. The experimental data lie much closer to our calculated values than to those of the EMM, without any exception. The experimental measurements on cluster samples with very narrow size distribution (diamonds and circles in Fig. 3 and diamonds in Fig. 4(c)[59]) are in better agreement with our calculations than the corresponding data from samples with broad size distribution. Finally, we provide evidence that spin-orbit coupling is important in wurtzite CdSe clusters and that some measured exciton energies correspond to higher energy B and C transitions than to the lowest energy A transition. Hence, EPM can be successfully used to study the implications of

TABLE V. The bulk parameters of semiconductor crystals. m_e and m_h are expressed in units of free electron mass m_0 and ϵ is unitless.

Compound	ϵ	m_e	m_h
CdS	7.06	0.19	0.80
CdSe	7.99	0.13	0.45
CdTe	8.65	0.09	0.72
AlP	9.80	0.21	0.94
GaP	9.10	0.10	0.86
GaAs	9.10	0.07	0.86
InP	10.9	0.08	0.58

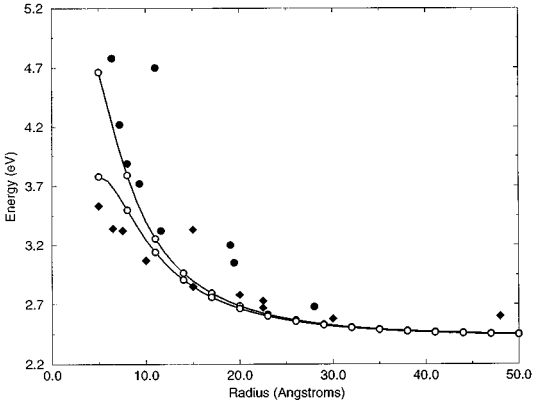

FIG. 3. Direct exciton energies of wurtzite (upper line) and zinc-blende (lower line) CdS spherical clusters compared with the experiments. Filled diamonds are used for the zinc-blende data points while filled circles represent the wurtzite clusters. These calculations employed 233 plane waves for the wurtzite and 283 plane waves for the zinc-blende structures.

valence-band splitting on the optical properties of quantum-confined nanocrystals.

B. CdTe clusters

Since both cadmium and tellurium are large atoms, CdTe clusters and crystals exist only in zinc-blende form. We also expect significant spin-orbit coupling in CdTe. Consequently, we have carried out band structure calculations on zinc-blende CdTe clusters using nonlocal EPM with the effects of spin-orbit coupling included in the Hamiltonian.[32] The parameters used in these calculations are given in Tables II and III. The spin-orbit coupling parameter μ was fit to the experimental spin-orbit splitting $\Delta=0.8$ eV at 300 K.[44]

Figure 5(a) presents the band structure for the zinc-blende CdTe crystal, while Fig. 5(b) compares the calculated direct exciton energies with the available experimental data.[60,61] The computational procedure employed is identical to that described above. The experimental spectral shifts (circles)[60] are added to our bulk value of 1.56 eV before plotting. As can be seen from the figure, the *A*, *B*, and *C* transitions in CdTe are much more separated in energy from each other than in systems with weaker spin-orbit coupling such as CdS and CdSe. Also, the *C* transition exhibits a stronger blueshift with decreasing cluster size than the *A* and *B* transitions. The experimental data[60,61] seem to match our *B* transitions very closely.

The absorption spectrum of an $R=10$ Å cluster sample in the experiments of Nozik and co-workers shows a prominent peak at 412 nm (3.01 eV). Upon close examination we also observe a shoulder at $\approx$428 nm (2.89 eV) that is masked by the more intense transition at 412 nm. Based on our calculations, we assign the 428 nm shoulder to *A* (up triangle) and the 412 nm peak [diamond in Fig. 5(b)] to a *B* transition. From the band structure displayed in Fig. 5(a) we also observe that the light-hole band is essentially a mirror image of the conduction band, and hence they both have similar effective masses. Consequently, the overlap of the electron-hole wavefunctions is much greater for *B* transitions than for *A*

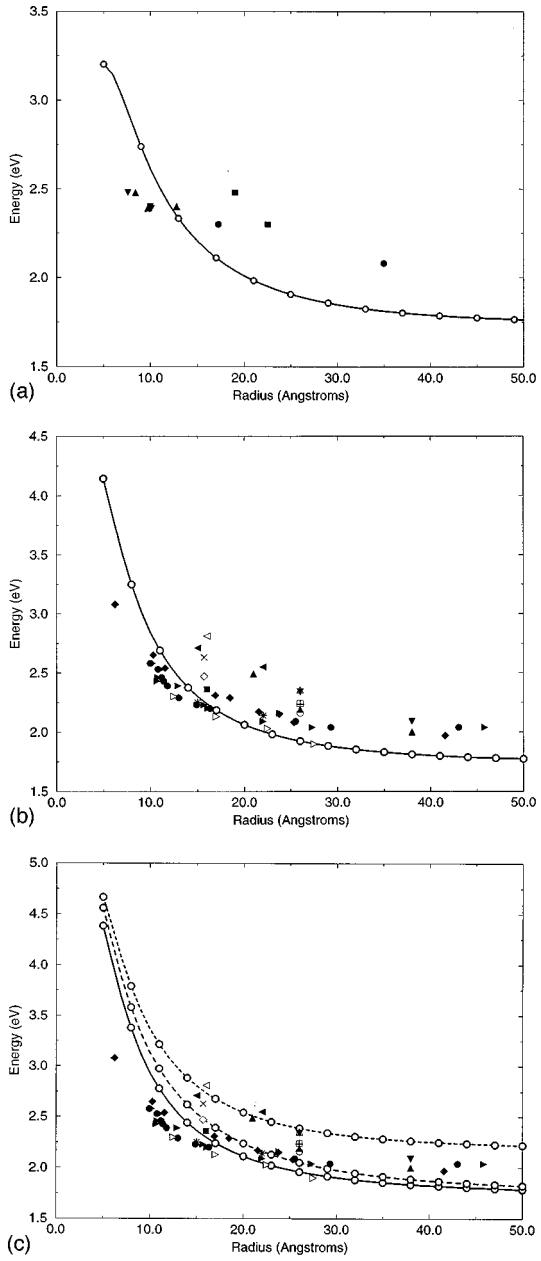

FIG. 4. (a) Direct exciton energies of zinc-blende CdSe clusters. Comparison is made with the available experimental data: circles;[50] squares;[51] up triangles (SAXS data from Ref. 52); down triangles (TEM data from Ref. 52). (b) Direct exciton energies of wurtzite CdSe clusters. Comparison is made with the available experimental data: filled square (heavy-hole datum from Ref. 25); open left triangle (split-off hole datum from Ref. 25); filled circles (SAXS data from Ref. 52); filled right triangles (TEM data from Ref. 52); open circle (heavy-hole datum from Ref. 53); open square (light-hole datum from Ref. 53); open diamond (heavy-hole datum from Ref. 54); $\times$ (light-hole/split-off-hole datum from Ref. 54); open right triangles;[55] stars (heavy-hole data from Ref. 56); filled left triangles (light-hole or split-off-hole data from Ref. 56); plus (heavy-hole datum from Ref. 57); open up triangle (light-hole datum from Ref. 57); filled up triangles (heavy-hole plus light hole data from Ref. 58); filled down triangles (split-off hole data from Ref. 58); filled diamonds.[59] (c) Calculated *A* (solid line), *B* (dashed line), and *C* (dotted line) transition energies, as discussed in the text. The experimental data are superimposed for comparison. The bulk transitions *A*, *B*, and *C* are at 1.79 eV, 1.81 eV, and 2.22 eV, respectively. The experimental spectral shifts are added to the bulk band gaps before plotting them.

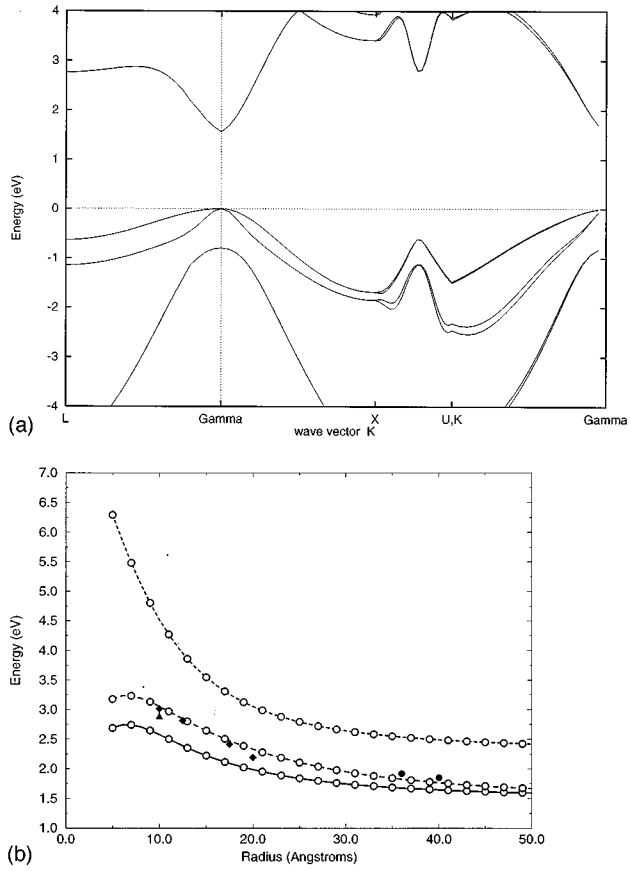

FIG. 5. (a) Band structure of a zinc-blende CdTe crystal obtained using nonlocal empirical pseudopotentials and 137 plane waves. Since EPM overestimates the bulk band gap by 0.085 eV, we shift the conduction bands by this amount before plotting. (b) Calculated transition energies *A* (solid), *B* (dashed), and *C* (dotted line) of zinc-blende CdTe clusters and comparison with the experimental data: circles;[60] triangle (heavy-hole datum from Ref. 60; diamonds[61]). The bulk transitions *A*, *B*, and *C* are at 1.56 eV, 1.56 eV, and 2.36 eV, respectively. The experimental spectral shifts are added to these band gaps before plotting them.

and *C* transitions. This is another reason why we assign the most intense peak in the experimental spectrum to the *B* transition.

C. AlP clusters

The binary semiconductor AlP is isoelectronic to Si_2 and they both crystallize in an identical lattice structure. Also, since Al and P are the nearest neighbors of Si in the periodic table, it is reasonable to expect that crystalline AlP will have electronic properties similar to that of bulk Si. Indeed that turns out to be true: both Si and AlP are indirect gap semiconductors with similar band structures. Likewise, since both these semiconductors are made of light elements, we expect spin-orbit coupling to be negligible in these crystals. We have reported on our investigation of the spectral shifts of silicon clusters before.[30] Now we present corresponding calculations on AlP clusters.

The previous calculated band structure of AlP was obtained using the LCAO-MO method and the corresponding

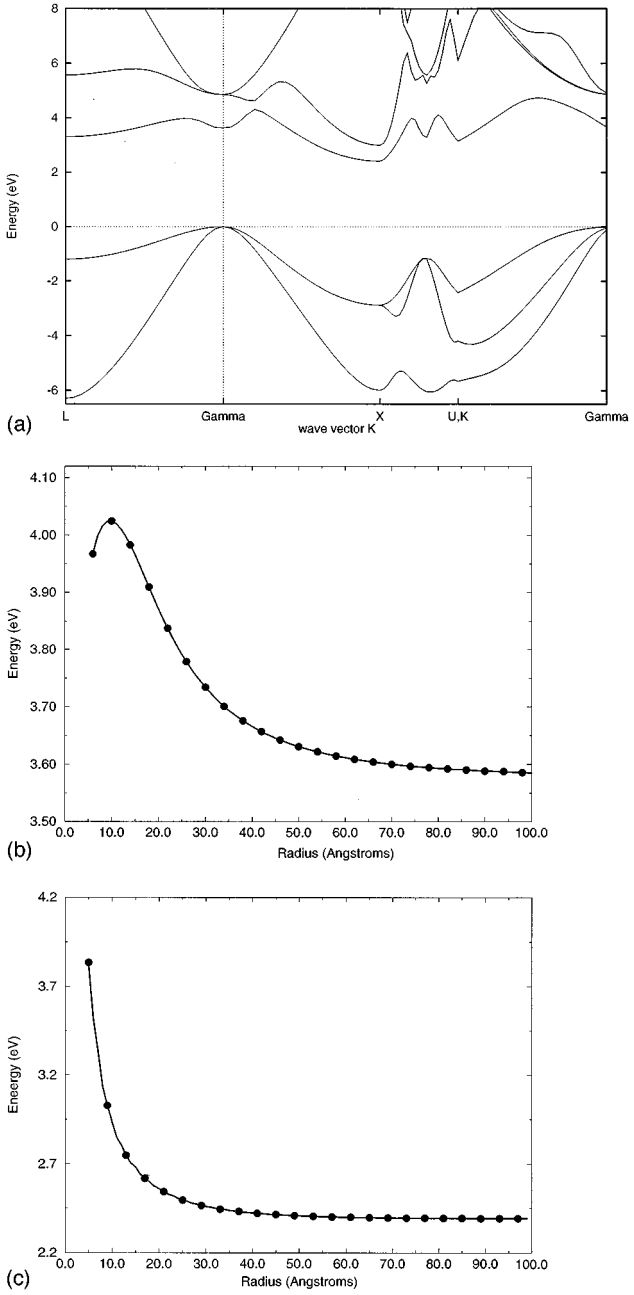

FIG. 6. (a) Band structure of a zinc-blende AlP crystal. (b) Direct and (c) indirect exciton energies of zinc-blende AlP clusters obtained using 283 plane waves.

band structure is not available from EPM calculations. Consequently, we have fitted the nonlocal parameters of AlP to reproduce the band structure calculated using the LCAO-MO method. Our initial guess for these parameters utilized the parameters of bulk Si.[30] In the end the optimal parameters gave 3.63 eV for the direct and 2.41 eV for the indirect gaps. These calculated values are in complete agreement with the corresponding experimental band gaps at 300 K.[62] Tables II–IV give the parameters, while Fig. 6 gives the bulk band structure and the calculated exciton energies of AlP clusters. Nanoscale AlP clusters have not been synthesized in the

laboratory so far. However, recent experimental efforts on Si clusters and porous Si[42] point to the possibility of similar interest on AlP clusters.

D. GaP and GaAs clusters

Figures 7(a) and 8(a) show the band structures of zinc-blende GaP and GaAs crystals obtained using the nonlocal (solid line) and the local (dashed line) empirical pseudopotentials, respectively. Tables II–IV show the parameters that were used in these calculations.[30,63] Comparison with the experimental data[64–67] clearly shows that the nonlocal approximation yields better band structures than does the local approximation.

The calculated band gaps of GaP, obtained using 283 plane waves and the local EPM method, are 2.79 eV for the direct transition and 2.15 eV for the indirect transition. The nonlocal EPM gives 2.88 and 2.17 eV, respectively, for these transitions. The corresponding experimental band gaps are 2.78 eV for the direct transition and 2.27 eV for the indirect transition.[62] For GaAs, the experimental direct gap is 1.47 eV, which is an average of the experimental band gaps at 0 and 300 K.[62] The calculated band gaps, obtained using 283 plane waves, are 1.50 eV with the local calculation and 1.52 eV with the nonlocal calculation.

The energy gap for a GaP cluster of radius $R=100$ Å, obtained using the local EPM method, is 2.83 eV for a direct transition, and 2.16 eV for an indirect transition. In order to obtain the experimental bulk gap we shifted the conduction bands by -0.05 eV for a direct transition, and $+0.11$ eV for an indirect transition. We carried out a similar correction when we used the nonlocal EPM method, shifting the conduction bands by -0.15 eV for the direct transition, and $+0.09$ eV for the indirect transition. The band gap of a GaAs cluster of radius $R=100$ Å has a fundamental gap of 1.54 eV in the local approximation, and 1.56 eV in the nonlocal approximation. In order to obtain the experimental bulk gap of 1.47 eV[62] we shifted the conduction bands by -0.07 eV and -0.09 eV, respectively, when we carried out cluster calculations using the local and the nonlocal pseudopotentials.

The exciton energies thus calculated are presented in Figs. 7 and 8. Since GaP is an indirect gap semiconductor, we present spectral shifts of both the direct and indirect transitions in Figs. 7(b) and 7(c), respectively. The results obtained from both local and nonlocal EPM are shown in these figures. Figure 7(b) also shows the comparison between our calculated exciton energies, and the recent experimental datum reported by Nozik and collaborators.[68] The position of their direct transition for a cluster of radius 15 Å is 2.95 eV while our nonlocal calculation predicts a value of 3.35 eV. At the moment the reason for this discrepancy is not understood.

From Figs. 7 and 8 it is clear that over a large range of cluster sizes the local EPM is able to reproduce spectral shifts as accurately as nonlocal EPM for both GaP and GaAs. However, at small cluster sizes the nonlocal correction on the spectral shifts is significant. At large cluster sizes the absorption spectrum shifts to higher energies with decreasing cluster size. This blueshift is expected due to confinement of the electron-hole pair in the cluster. However, at small cluster sizes the absorption spectra of GaAs clusters shift to lower energies with decreasing cluster size; a trend opposite to that observed for large clusters. In the case of GaP, which is an indirect gap semiconductor, the lowest energy transition exhibits the expected blueshift at both large and small cluster sizes. But this transition is not observable because it is forbidden. The origin of the absorption spectrum, corresponding to the observable direct transition, shifts to lower energies with decreasing cluster size at small cluster sizes. Both local and nonlocal pseudopotentials exhibit the same qualitative behavior. The main difference is that the nonlocal EPM predicts less redshift in small clusters than the local EPM.

We can explain the calculated trends in the following way. At large cluster sizes the electron and hole are both confined in a spherical well. This quantum confinement increases the band gap with decreasing cluster size and it is the dominant effect in this size regime. In these large clusters, the negatively charged electron and the positively charged hole are spatially separated and hence the Coulomb attraction between them is negligible. However, in small clusters the Coulomb attraction energy between the electron-hole pair cannot be neglected. While the band gap still increases with decreasing cluster size, in small clusters this increase is sufficiently overcome by the Coulomb energy that the spectra shift to lower energies. For example, in a $R=10$ Å cluster the band gap and Coulomb term are 3.78 and -0.28 eV, respectively, while in a $R=5$ Å cluster the corresponding energies are 3.80 and -0.57 eV, respectively. This demonstrates the importance of Coulomb attraction on the exciton energies in small crystalline quantum dots. Increasingly experimental evidence seems to point to the ability to synthesize such nanocrystalline materials with passivating surface ligands. Consequently, in the small cluster size regime the absorption spectra of clusters may exhibit redshift instead of the blueshift.

At present enough reliable experimental data are not available for the spectral shifts of these important IIIA-VB semiconductor clusters, because of considerable experimental difficulties that arise in trying to synthesize IIIA-VB semiconductor clusters with narrow size distribution. However, based on our experience with CdS, CdSe, CdTe, and InP clusters (see below), we expect our calculated spectral shifts of AIP, GaP, and GaAs clusters to be good estimates of the expected spectral shifts.

E. InP clusters

Nozik and co-workers have succeeded in synthesizing InP clusters and for the first time showed an exciton transition in the spectrum of a III-V quantum dot.[69] The present work compares their experimental results with our theoretical predictions. We used the same procedure as before: First, we found the parameters of the EPM Hamiltonian and then calculated the excitonic energies of InP clusters. The band structure calculations on zinc-blende InP crystal were carried

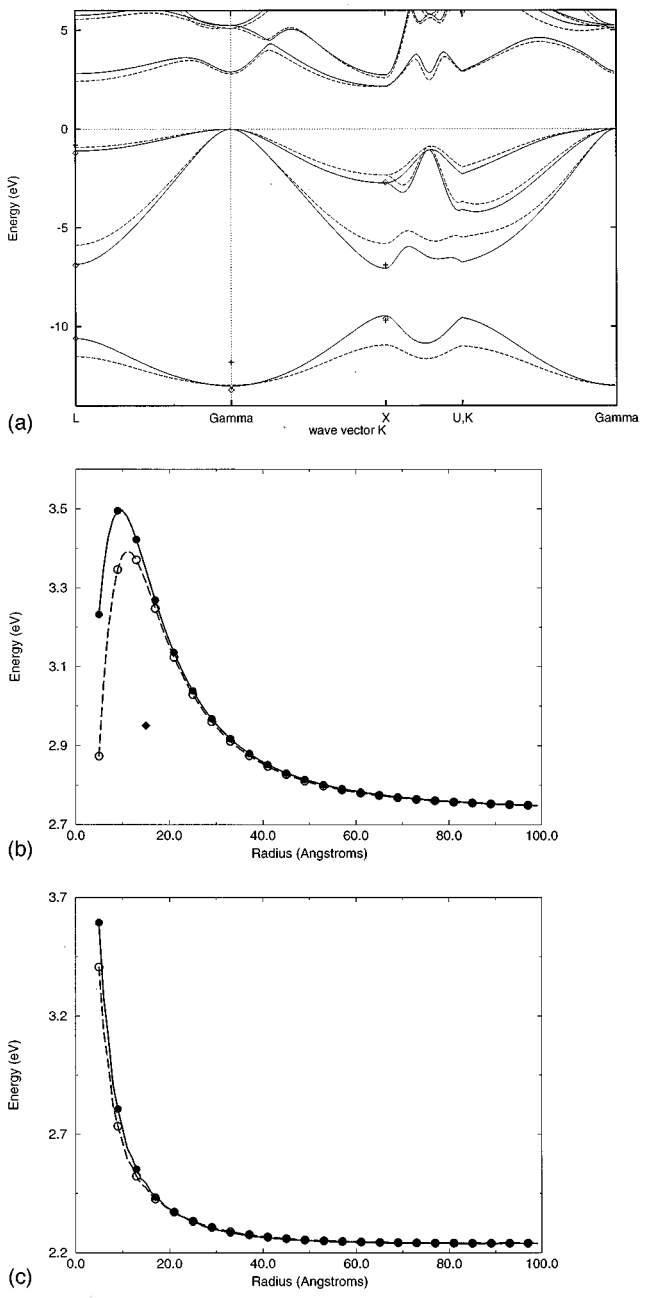

FIG. 7. (a) Band structure of a zinc-blende GaP crystal obtained using 283 plane waves. Comparison between the nonlocal (solid line) and the local (dashed line) empirical pseudopotential approximations is made. Experimental data are superimposed on the band structure: diamonds;[64] plus symbols.[65] The nonlocal pseudopotential calculations are seen to agree better with the experimental data than the local pseudopotential calculations. (b) Direct exciton energies of zinc-blende GaP clusters. The open circles are obtained using local pseudopotentials and filled circles are obtained using nonlocal pseudopotentials. Comparison is made with the available experimental datum: diamond.[68] (c) Indirect exciton energies of zinc-blende GaP clusters. The open circles are obtained using local pseudopotentials and filled circles are obtained using nonlocal pseudopotentials.

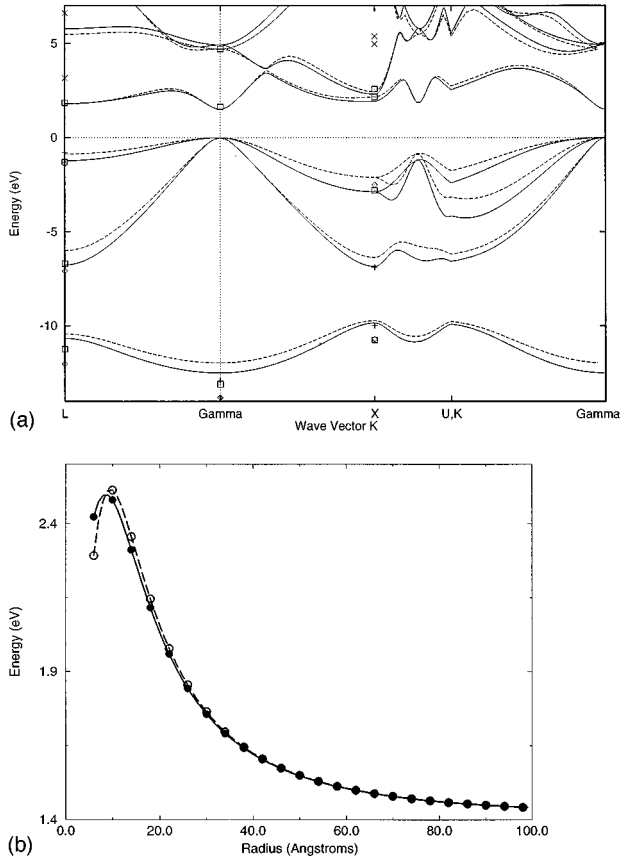

FIG. 8. (a) Band structure of a zinc-blende GaAs crystal. Comparison between the nonlocal (solid line) and the local (dashed line) empirical pseudopotential approximations is made. Experimental data are superimposed on the band structure: diamonds;[64] plus symbols;[65] $\times$ symbols;[66] squares.[67] The nonlocal pseudopotential calculations agree better with the experimental data than the local calculations. (b) Direct exciton energies of GaAs spherical clusters obtained using 283 plane waves. The open circles are obtained using local pseudopotentials and filled circles are obtained using nonlocal pseudopotentials.

out using the nonlocal EPM that includes the effects of spin-orbit coupling. The parameters we employ are slightly different from those used by Chelikowsky, but otherwise the two calculations give nearly identical band structures. Complete set of parameters used in our calculations are tabulated in Tables II and III.

Figure 9(a) displays the band structure of bulk InP and Fig. 9(b) presents the exciton energies of the clusters as a function of their radius. The calculated A, B, and C transition energies of zinc-blende InP clusters are shifted by -0.21 eV, -0.24 eV, and -0.23 eV, respectively, so that these energies for a cluster of $R=100$ Å agree with the corresponding bulk values of 1.35, 1.35, and 1.56 eV.[62]

The type (a) sample in the experiments of Nozik and co-workers have a radius of about 20 Å and exhibits an exciton transition at about 1.7 eV.[69] This paper quotes 0.35 eV blueshift for the onset of absorption for this colloidal sample whose mean diameter is 26.1 Å. However, 0.35 eV is not the blueshift for a particle with a diameter of 26.1 Å because colloid (a) has a broad size distribution with a standard deviation of 7.5 Å (see Fig. 3 of Ref. 69). Thus the onset of absorption for this sample really corresponds to a size of about 40 Å in diameter.[69] We use this value for the particle

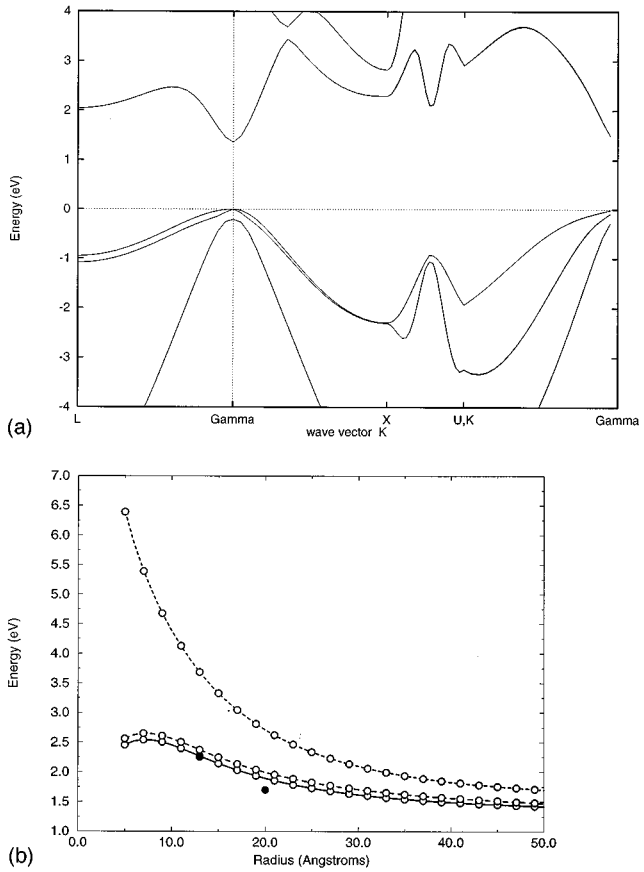

FIG. 9. (a) Band structure of a zinc-blende InP crystal obtained using nonlocal empirical pseudopotentials and 137 plane waves. Since EPM overestimates the bulk band gap by 0.16 eV, we shift the conduction bands by this amount before plotting. (b) Calculated transition energies *A* (solid), *B* (dashed), and *C* (dotted line) of zinc-blende InP clusters and comparison with the experimental data: circles.[69] The bulk transitions *A*, *B*, and *C* are 1.35 eV, 1.35 eV, and 1.56 eV, respectively. The experimental spectral shifts are added to these band gaps before plotting them.

size while comparing experimental blueshift with our calculations. The difference between our calculated exciton energy and the experimental value is approximately 0.19 eV.

The type (c) sample has a radius of 13 Å and the exciton transition is at 2.25 eV, in perfect agreement with our calculation. From this comparison it is clear that the overall trend of the experimental spectral shifts is in close agreement with our calculations. Additional reliable data on spectral shifts over a range of cluster sizes will certainly be useful in further establishing the accuracy of our calculations.

Our band structure calculations on all IIIA-VB semiconductor clusters suggest that local empirical pseudopotentials are reasonably accurate compared to the nonlocal empirical pseudopotentials for the calculations of the spectral shifts of these clusters. The nonlocal corrections on the spectral shifts are most important in small cluster sizes. In addition, our calculations have shown that, while quantum confinement energy is the dominant factor affecting spectral shifts in large clusters, the Coulomb interaction between the electron and hole has a significant effect in small clusters. The attractive Coulomb interaction is sufficiently strong in small clusters that it overcomes the confinement energy of the electron-hole pair and gives rise to redshift, instead of the blueshift, of the electronic absorption spectrum.

VI. SUMMARY

In summary, we have calculated the spectral shifts of CdS, CdSe, CdTe, AlP, GaP, GaAs, and InP semiconductor clusters using the most accurate available empirical pseudopotentials. These semiconductors cover a wide range of bond polarities and band structures. These binary clusters also represent a series in which one ion is held constant while the other ion is varied along a column of the periodic table. Furthermore, the pseudopotentials employed in these calculations incorporate the effects of nonlocality and spin-orbit coupling whenever they are important. At present these calculations represent the most sophisticated calculations on the spectral shifts of semiconductor clusters.

We find that for zinc-blende CdS, wurtzite CdS, wurtzite CdSe, zinc-blende CdTe, and zinc-blende InP clusters the spectral shifts calculated using our band structure model are in excellent agreement with experiments. The shapes and crystal structures of the unit cell have significant effect on the exciton energies. The small clusters in particular are sensitive to whether their crystal structure is zinc-blende or wurtzite. In the case of small CdS clusters where the experimental data on lattice structure are either ambiguous or unavailable, our calculations are able to assign the structure unambiguously. While reliable experimental data are not yet available for zinc-blende CdSe clusters, we predict these clusters also to exhibit similar sensitivity to crystal structure.

In the absence of experimental data on AlP, GaP, and GaAs clusters, our calculations provide reasonable estimates of the expected spectral shifts and trends in these clusters as a function of cluster size. The very little difference between the local and the nonlocal calculations confirms the validity of the local pseudopotential method for the calculations of the exciton energies. The main effect of the nonlocal pseudopotentials seems to be to reduce the magnitude of the redshift seen in the spectral shifts of some small IIIA-VB semiconductor clusters. Similarly, the spin-orbit interaction does not change the lowest exciton energies. The main effect of the spin-orbit interaction is to split the valence band into *A*, *B*, and *C* sub-bands, thus giving rise to new transitions in the spectra. We provide evidence that transitions originating from spin-orbit split valence sub-bands are being observed even in nanoscale CdSe clusters. This explains the reasons for considerable scatter in the experimentally determined exciton energies for a given cluster size. We also assign the observed transitions in CdTe clusters to *B* transitions. This study, together with our previous investigation, provides evidence that the empirical pseudopotential method yields unique insights into the quantum confinement effects and is a powerful quantitative tool for calculating the spectral shifts of semiconductor clusters.

ACKNOWLEDGMENTS

This research is supported by the New York University and the Donors of The Petroleum Research Fund (ACS-PRF # 30906-AC), administered by the American Chemical Society. We are grateful to A. P. Alivisatos and Moungi Bawendi for communicating their beautiful experimental data of Fig. 4 in this paper.

APPENDIX: LOCAL PSEUDOPOTENTIALS OF WURTZITE STRUCTURE CRYSTALS

The local pseudopotential (V_L) experienced by a valence electron at a point $\mathbf{r}$ inside a crystal lattice is given by

$$V_L(\mathbf{r})=\sum_{\mathbf{R},j} v_j(\mathbf{r}-\mathbf{R}-\mathbf{d}_j), \tag{A1}$$

where the summation is over all the basis atoms j at each lattice point $\mathbf{R}$, and v_j is the atomic pseudopotential due to the jth basis atom at the lattice site $\mathbf{R}$. Fourier expansion of v_j yields

$$V_L(\mathbf{r})=\frac{1}{Nn_a}\sum_{\mathbf{G}}\sum_{\mathbf{R},j} v_j(\mathbf{G})\exp[i\mathbf{G}\cdot(\mathbf{r}-\mathbf{R}-\mathbf{d}_j)], \tag{A2}$$

where N are the number of unit cells and n_a are the number of basis atoms per unit cell.

The wurtzite crystals are made of two interpenetrating hexagonal close packed (hcp) lattices. One hcp lattice is entirely made of A type atoms and the other entirely of B type atoms ($A\neq B$) and these two lattices are displaced from each other by $2t_2=3/8c_0$ along the c-axis. However, the hcp lattice is not a Bravais lattice. The hcp lattice consists of two interpenetrating simple hexagonal Bravais lattices, displaced from one another by $2t_1=(1/3\mathbf{a}_1,1/3\mathbf{a}_2,1/2\mathbf{a}_3)$, where $(\mathbf{a}_1,\mathbf{a}_2,\mathbf{a}_3)$ are the direct lattice primitive translation vectors of the simple hexagonal Bravais lattice. Hence, the wurtzite structure is a network of four simple hexagonal lattices, with four atoms per unit cell and two different types of atoms. We associate atom sites (1,3) and (2,4) with A and B type atoms, respectively. For this case $n_a=4$ and the position vectors of the four basis atoms in the unit cell are given by

$$\mathbf{d}_1=-(\mathbf{t}_1+\mathbf{t}_2), \tag{A3}$$

$$\mathbf{d}_2=-(\mathbf{t}_1-\mathbf{t}_2), \tag{A4}$$

$$\mathbf{d}_3=(\mathbf{t}_1-\mathbf{t}_2), \tag{A5}$$

$$\mathbf{d}_4=(\mathbf{t}_1+\mathbf{t}_2). \tag{A6}$$

The local pseudopotential of the valence electron interacting with a periodic wurtzite lattice is given by

$$V_L(\mathbf{r})=\sum_{\mathbf{G}}\left[\frac{1}{n_a}\sum_j v_j(\mathbf{G})\exp(-i\mathbf{G}\cdot\mathbf{d}_j)\right]\exp(i\mathbf{G}\cdot\mathbf{r}) \tag{A7}$$

$$=\sum_{\mathbf{G}}\frac{1}{n_a}\{v_1(\mathbf{G})[\exp(-i\mathbf{G}\cdot\mathbf{d}_1)+\exp(-i\mathbf{G}\cdot\mathbf{d}_3)] + v_2(\mathbf{G})[\exp(-i\mathbf{G}\cdot\mathbf{d}_2)+\exp(-i\mathbf{G}\cdot\mathbf{d}_4)]\} \times\exp(i\mathbf{G}\cdot\mathbf{r}), \tag{A8}$$

since atoms 1 and 3 (A atoms), and 2 and 4 (B atoms) are identical in the wurtzite lattice. Defining symmetric and antisymmetric form factors as

$$V_S(\mathbf{G})=\tfrac{1}{2}[v_1(\mathbf{G})+v_2(\mathbf{G})],$$
$$V_A(\mathbf{G})=\tfrac{1}{2}[v_1(\mathbf{G})-v_2(\mathbf{G})], \tag{A9}$$

and rewriting v_1 and v_2 in terms of V_S and V_A we obtain

$$V_L(\mathbf{r})=\sum_{\mathbf{G}}[V_S(\mathbf{G})S_S(\mathbf{G})+iV_A(\mathbf{G})S_A(\mathbf{G})]\exp(i\mathbf{G}\cdot\mathbf{r}), \tag{A10}$$

where the symmetric (S_S) and anti-symmetric (S_A) structure factors are given by

$$S_S(\mathbf{G})=\frac{1}{n_a}\sum_j \exp(-i\mathbf{G}\cdot\mathbf{d}_j),$$
$$S_A(\mathbf{G})=\frac{-i}{n_a}\sum_j P_j\exp(-i\mathbf{G}\cdot\mathbf{d}_j), \tag{A11}$$

with $P_j=(-1)^{j+1}$. Thus the pseudopotentials of wurtzite and zinc-blende crystals differ from each other only in the definition of the structure factors. We can carry out the summations in Eq. (A11) as follows.

The hexagonal lattice is characterized by three parameters: a_0, c_0, and u_0. Like zinc-blende, wurtzite lattice has tetrahedral coordination about each ion, but the orientation of the tetrahedron is different from that of zinc-blende. If we assume perfect tetrahedral coordination, then

$$\frac{c_0}{a_0}=\sqrt{\frac{8}{3}}=\frac{1}{\sqrt{u_0}},\quad u_0=0.375=\frac{3}{8}. \tag{A12}$$

The direct lattice primitive translation vectors of the simple hexagonal Bravais lattice are[70]

$$\mathbf{a}_1=(1,0,0)a_0,\quad \mathbf{a}_2=\left(\frac{1}{2},\frac{\sqrt{3}}{2},0\right)a_0,$$
$$\mathbf{a}_3=\left(0,0,\frac{c_0}{a_0}\right)a_0=\left(0,0,\frac{1}{\sqrt{u_0}}\right)a_0. \tag{A13}$$

With this definition, the position vectors of the basis atoms are

$$\mathbf{d}_1=-\frac{1}{4}\left[1,\frac{1}{\sqrt{3}},(1+2u_0)\frac{c_0}{a_0}\right]a_0, \tag{A14}$$

$$\mathbf{d}_2 = -\frac{1}{4}\left[1, \frac{1}{\sqrt{3}}, (1-2u_0)\,\frac{c_0}{a_0}\right]a_0, \tag{A15}$$

$$\mathbf{d}_3 = \frac{1}{4}\left[1, \frac{1}{\sqrt{3}}, (1-2u_0)\,\frac{c_0}{a_0}\right]a_0, \tag{A16}$$

$$\mathbf{d}_4 = \frac{1}{4}\left[1, \frac{1}{\sqrt{3}}, (1+2u_0)\,\frac{c_0}{a_0}\right]a_0, \tag{A17}$$

in Cartesian coordinate representation.

In the zinc-blende crystal the nearest neighbor atoms are located half-way along the face diagonal of the fcc lattice. Consequently, if $a_0(zb)$ is the lattice constant of the zinc-blende crystal, then the nearest neighbor distance is

$$r_n(\mathrm{zb}) = \frac{1}{\sqrt{2}}\,a_0(\mathrm{zb}). \tag{A18}$$

In the wurtzite crystal, the nearest neighbor atoms are located along the edges of the hexagon. Consequently,

$$r_n(\mathrm{wz}) = a_0(\mathrm{wz}). \tag{A19}$$

Since $r_n(\mathrm{zb}) = r_n(\mathrm{wz})$, comparing Eqs. (A18) and (A19) we obtain the relation

$$a_0(\mathrm{zb}) = \sqrt{2}\,a_0(\mathrm{wz}) \tag{A20}$$

and

$$\mathbf{G}_{\mathrm{wz}} = \mathbf{G}_{\mathrm{zb}}, \tag{A21}$$

$$= \frac{2\pi}{a_0(\mathrm{zb})}\,(G_x, G_y, G_z), \tag{A22}$$

$$= \frac{\sqrt{2}\pi}{a_0(\mathrm{hex})}\,(G_x, G_y, G_z). \tag{A23}$$

This definition allows the comparison of **G** vectors of zinc-blende and wurtzite crystals on an equal footing.

Substituting Eqs. (A3)–(A5) into (A11) and carrying out some algebraic manipulations we obtain

$$\begin{aligned} S_S(\mathbf{G}) &= \cos(\mathbf{G}\cdot\mathbf{t}_1)\cos(\mathbf{G}\cdot\mathbf{t}_2), \\ S_A(\mathbf{G}) &= \cos(\mathbf{G}\cdot\mathbf{t}_1)\sin(\mathbf{G}\cdot\mathbf{t}_2), \end{aligned} \tag{A24}$$

where

$$\mathbf{t}_1 = \frac{1}{6}\,(\mathbf{a}_1+\mathbf{a}_2) + \frac{\mathbf{a}_3}{4} = \left(\frac{1}{4}, \frac{1}{\sqrt{48}}, \frac{1}{\sqrt{6}}\right)a_0, \tag{A25}$$

$$\mathbf{t}_2 = \frac{1}{2}\,u_0\mathbf{a}_3 = \left(0,0, \frac{\sqrt{u_0}}{2}\right)a_0. \tag{A26}$$

Finally, substituting Eqs. (A23), (A25), and (A26) into Eq. (A24) we obtain

$$S_S(\mathbf{G}) = \cos\left[\sqrt{2}\,\pi\left(\frac{G_x}{4} + \frac{G_y}{\sqrt{48}} + \frac{G_z}{\sqrt{6}}\right)\right] \times \cos\left(\sqrt{2}\,\pi G_z\,\frac{\sqrt{u_0}}{2}\right), \tag{A27}$$

$$S_A(\mathbf{G}) = \cos\left[\sqrt{2}\,\pi\left(\frac{G_x}{4} + \frac{G_y}{\sqrt{48}} + \frac{G_z}{\sqrt{6}}\right)\right] \times \sin\left(\sqrt{2}\,\pi G_z\,\frac{\sqrt{u_0}}{2}\right). \tag{A28}$$

We can also define **G** as

$$\mathbf{G} = (l\mathbf{b}_1, m\mathbf{b}_2, n\mathbf{b}_3), \tag{A29}$$

where $\mathbf{b}_1$, $\mathbf{b}_2$, and $\mathbf{b}_3$ are the reciprocal lattice primitive translational vectors given by

$$\begin{aligned} \mathbf{b}_1 &= \frac{\sqrt{2}\pi}{a_0}\left(\sqrt{2}, -\sqrt{\frac{2}{3}}, 0\right), \quad \mathbf{b}_2 = \frac{\sqrt{2}\pi}{a_0}\left(0, \sqrt{\frac{8}{3}}, 0\right), \\ \mathbf{b}_3 &= \frac{\sqrt{2}\pi}{a_0}\left(0,0, \frac{\sqrt{2}a_0}{c_0}\right). \end{aligned} \tag{A30}$$

Substituting Eqs. (A30) and (A29) into (A11), utilizing the relations

$$\mathbf{b}_i\cdot\mathbf{a}_i = 2\pi, \quad \mathbf{b}_i\cdot\mathbf{a}_j = 0 \quad (i \neq j), \tag{A31}$$

and carrying out some algebraic manipulations, we obtain

$$\begin{aligned} S_S(\mathbf{G}) &= \cos\left[2\pi\left(\frac{l}{6} + \frac{m}{6} + \frac{n}{4}\right)\right]\cos(n\pi u_0), \\ S_A(\mathbf{G}) &= \cos\left[2\pi\left(\frac{l}{6} + \frac{m}{6} + \frac{n}{4}\right)\right]\sin(n\pi u_0). \end{aligned} \tag{A32}$$

Equations (A27)–(A28) and (A32) are equivalent. We find that the above structure factors yield band structures in excellent agreement with those of Cohen and Bergstresser for wurtzite crystals.[43] We tested our program with both these structure factors and verified that they give identical band structures.

Previously we used a different coordinate system for the definition of the direct lattice vectors of the simple hexagonal Bravais lattice.[30] That definition resulted in structure factors different from the ones given above. While these two definitions are equivalent in principle, in practice the values of the parameters V_S and V_A are intimately linked to the choice of the coordinate system and the structure factors determined therefrom. The present choice of the coordinate system that gives rise to the structure factors in Eqs. (A27)–(A28) and (A32) yield correct band structures, in complete agreement with the original band structures of Cohen and Bergstresser.[43]

[1] R. Pool, Science **248**, 1186 (1990).
[2] E. Corcoran, Sci. Am. **263**, 122 (1990).
[3] S. Bjornholm, Contemp. Phys. **31**, 309 (1990).
[4] L. E. Brus, J. Phys. Chem. **90**, 2555 (1986); M. L. Steigerwald and L. E. Brus, Acc. Chem. Res. **23**, 183 (1990); M. G. Bawendi, M. L. Steiger-

wald, and L. E. Brus, Annu. Rev. Phys. Chem. **41**, 477 (1990).
[5] Y. Wang, A. Suna, W. Mahler, and R. Kasowsky, J. Chem. Phys. **87**, 7315 (1987); Y. Wang and N. Herron, J. Phys. Chem. **95**, 525 (1991); Y. Wang, *ibid*. **95**, 1119 (1991).
[6] J. L. Elkind, J. M. Alford, F. D. Weiss, R. T. Laaksonen, and R. E. Smalley, J. Chem. Phys. **87**, 2397 (1987); S. Maruyama, L. R. Anderson, and R. E. Smalley, *ibid*. **93**, 5349 (1990); J. M. Alford, R. T. Laaksonen, and R. E. Smalley, *ibid*. **94**, 2618 (1991); L. R. Anderson, S. Maruyama, and R. E. Smalley, Chem. Phys. Lett. **176**, 348 (1991).
[7] E. Kaxiras and K. C. Pandey, Phys. Rev. B **38**, 12736 (1988).
[8] E. Kaxiras, Chem. Phys. Lett. **163**, 323 (1989); Phys. Rev. Lett. **64**, 551 (1990).
[9] B. C. Bolding and H. C. Andersen, Phys. Rev. B **41**, 10568 (1990).
[10] D. A. Jelski, B. L. Swift, T. T. Rantala, X. Xia, and T. F. George, J. Chem. Phys. **95**, 8552 (1991); B. L. Swift, D. A. Jelski, D. S. Higgs, T. T. Rantala, and T. F. George, Phys. Rev. Lett. **66**, 2686 (1991).
[11] J. P. Proot, C. Delerue, and G. Allan, Appl. Phys. Lett. **61**, 1948 (1992); J. P. Proot, C. Delerue, G. Allan, and M. Lannoo, Appl. Surf. Sci. **65**, 423 (1993).
[12] B. Delley and E. F. Steigmeier, Phys. Rev. B **47**, 1397 (1993).
[13] M. O'Neil, J. Marohn, and G. McLendon, J. Phys. Chem. **94**, 4356 (1990).
[14] L. M. Ramaniah and S. V. Nair, Phys. Rev. B **47**, 7132 (1992).
[15] S. B. Zhang, C. Y. Yeh, and A. Zunger, Phys. Rev. B **48**, 11204 (1993); L. W. Wang and A. Zunger, J. Chem. Phys. **100**, 2394 (1994); L. W. Wang and A. Zunger, in *Nanocrystalline Semiconductor Materials*, edited by P. V. Kamat and D. Meisel (Elsevier Science, New York, 1996).
[16] N. A. Hill and K. B. Whaley, J. Chem. Phys. **100**, 2831 (1994).
[17] M. G. Bawendi, A. R. Kortan, M. L. Steigerwald, and L. E. Brus, J. Chem. Phys. **91**, 7282 (1989).
[18] J. J. Shiang, A. N. Goldstein, and A. P. Alivisatos, J. Chem. Phys. **92**, 3232 (1990); V. L. Colvin, A. P. Alivisatos, and J. G. Tobin, Phys. Rev. Lett. **66**, 2786 (1991); M. A. Olshavsky, A. N. Goldstein, and A. P. Alivisatos, J. Am. Chem. Soc. **112**, 9438 (1990).
[19] Y. Z. Hu, S. W. Koch, M. Lindberg, N. Peyghambarian, E. L. Pollock, and F. F. Abraham, Phys. Rev. Lett. **64**, 1805 (1990); Y. Z. Hu, S. W. Koch, and D. B. T. Thoai, Mod. Phys. Lett. B **4**, 1009 (1990); L. Wang, L. P. F. Chibante, F. K. Tittel, R. F. Curl, and R. E. Smalley, Chem. Phys. Lett. **172**, 335 (1990).
[20] L. T. Canham, Appl. Phys. Lett. **57**, 1046 (1990); A. G. Callis and L. T. Canham, Nature **353**, 335 (1991); V. Lehmann and U. Gösele, Appl. Phys. Lett. **58**, 856 (1991); A. J. Read, R. J. Needs, K. J. Nash, L. T. Canham, P. D. J. Calcott, and A. Qteish, Phys. Rev. Lett. **69**, 1232 (1992); M. Stutzmann, M. S. Brandt, M. Rosenbauer, and J. Weber, Phys. Rev. B **47**, 4806 (1993).
[21] K. Raghavachari and V. Logovinsky, Phys. Rev. Lett. **55**, 2853 (1985); K. Raghavachari, J. Chem. Phys. **83**, 3520 (1985); *ibid*. **84**, 5672 (1986); K. Raghavachari and C. M. Rohlfing, Chem. Phys. Lett. **143**, 428 (1988); J. Chem. Phys. **89**, 2219 (1989); C. M. Rohlfing and K. Raghavachari, Chem. Phys. Lett. **167**, 559 (1990).
[22] R. Biswas and D. R. Hamann, Phys. Rev. Lett. **55**, 2001 (1985); Phys. Rev. B **36**, 6434 (1987); I. Kwon, R. Biswas, and C. M. Soukoulis, *ibid.* **45**, 3332 (1992).
[23] J. Tersoff, Phys. Rev. Lett. **56**, 632 (1986); Phys. Rev. B **37**, 6991 (1988); *ibid*. **38**, 9902 (1988).
[24] D. Tomanek and M. A. Schlüter, Phys. Rev. B **36**, 1208 (1987).
[25] M. G. Bawendi, W. L. Wilson, L. Rothberg, P. J. Carroll, T. M. Jedju, M. L. Steigerwald, and L. E. Brus, Phys. Rev. Lett. **65**, 1623 (1990).
[26] M. Menon and R. E. Allen, Phys. Rev. B **38**, 6196 (1988); M. Menon and K. R. Subbaswamy, Phys. Rev. Lett. **67**, 3487 (1991).
[27] A. D. Yoffe, Adv. Phys. **42**, 173 (1993).
[28] R. Rossetti, S. Nakahara, and L. E. Brus, J. Chem. Phys. **79**, 1086 (1983).
[29] W. L. Wilson, P. F. Szajowski, and L. E. Brus, Science **262**, 1242 (1993).
[30] M. V. Ramakrishna and R. A. Friesner, Phys. Rev. Lett. **67**, 629 (1991); J. Chem. Phys. **95**, 8309 (1991); *ibid*. **96**, 873 (1992); SPIE Proc. **1599**, 85 (1992); Isr. J. Chem. **33**, 3 (1993); B. Zorman, M. V. Ramakrishna, and R. A. Friesner, J. Phys. Chem. **99**, 7649 (1995).
[31] P. E. Lippens and M. Lannoo, Phys. Rev. B **41**, 6079 (1990).
[32] J. R. Chelikowsky and M. L. Cohen, Phys. Rev. B **14**, 556 (1976).
[33] H. A. Bethe and E. E. Salpeter, *Quantum Mechanics of One and Two Electron Atoms* (Springer-Verlag, Berlin, 1957).
[34] J. P. Walter, M. V. Cohen, V. Petroff, and M. Balkanski, Phys. Rev. B **1**, 2661 (1970).
[35] F. Herman and S. Skillman, *Atomic Structure Calculation* (Prentice–Hall, Englewood Cliffs, NJ, 1963).
[36] W. A. Harrison, *Solid State Theory* (Dover, New York, 1980), Chap. 8.
[37] J. C. Phillips, *Bonds and Bands in Semiconductors* (Academic, 1973).
[38] N. Peyghambarian, S. W. Koch, and A. Mysyrowicz, *Introduction to Semiconductor Optics* (Prentice–Hall, Englewood Cliffs, NJ, 1993).
[39] A. Franceschetti and A. Zunger (unpublished).
[40] S. Flügge, *Practical Quantum Mechanics* (Springer-Verlag, Berlin, 1971).
[41] Y. Kayanuma, Phys. Rev. B **38**, 9797 (1988).
[42] K. A. Littau, P. J. Szajowski, A. J. Muller, A. R. Kortan, and L. E. Brus, J. Phys. Chem. **97**, 1224 (1993).
[43] T. K. Bergstresser and M. L. Cohen, Phys. Rev. **164**, 1069 (1967).
[44] O. Madelung, *Semiconductors Other Than Group IV Elements and III-V Compounds* (Springer-Verlag, Berlin, 1992).
[45] Y. R. Wang and C. B. Duke, Phys. Rev. B **37**, 6417 (1988).
[46] R. Rossetti, J. L. Ellison, J. M. Gibson, and L. E. Brus, J. Chem. Phys. **80**, 4464 (1984).
[47] N. Chestnoy, T. D. Harris, R. Hull, and L. E. Brus, J. Phys. Chem. **90**, 3393 (1985).
[48] Y. Wang and N. Herron, Phys. Rev. B **42**, 7253 (1990).
[49] T. Vossmeyer, L. Katsikas, M. Giersig, I. G. Popovic, K. Diesner, A. Chemseddine, A. Eychmüller, and H. Weller, J. Phys. Chem. **98**, 7665 (1994).
[50] G. Hodes, A. Albu-Haron, F. Decker, and P. Motisuke, Phys. Rev. B **36**, 4215 (1987).
[51] A. P. Alivisatos, A. L. Harris, N. J. Levinos, M. L. Steigerwald, and L. E. Brus, J. Chem. Phys. **89**, 4001 (1988).
[52] J. E. Bowen Katari, V. L. Colvin, and A. P. Alivisatos, J. Phys. Chem. **98**, 4109 (1994).
[53] S. H. Park, R. A. Morgan, Y. Z. Hu, M. Lindberg, and N. Peyghambarian, J. Opt. Soc. Am. B **7**, 2097 (1990).
[54] U. Woggon, M. Müller, U. Lembke, I. Rückmann, and J. Česnulevicius, Superlatt. Microstruct. **9**, 245 (1991).
[55] N. Nogami, S. Suzuki, and K. Nagasaka, J. Non Cryst. Solids **135**, 182 (1991).
[56] N. F. Borrelli, D. W. Hall, H. J. Holland, and D. W. Smith, J. Appl. Phys. **61**, 5399 (1987).
[57] N. Peyghambarian, B. Fluegel, D. Hulin, A. Migus, M. Joffre, A. Antonetti, S. W. Koch, and M. Lindberg, IEEE J. Quantum Electron. **25**, 2516 (1989).
[58] A. I. Ekimov, F. Hache, M. C. Schanne-Kleine, D. Ricard, C. Flytzanis, I. A. Kudryavstev, T. V. Yazeva, A. V. Rodina, and A. L. Efros, J. Opt. Soc. Am. B **10**, 100 (1993).
[59] C. B. Murray, D. J. Norris, and M. G. Bawendi, J. Am. Chem. Soc. **115**, 8706 (1993).
[60] V. Esch, B. Fluegel, G. Khitrova, H. M. Gibbs, X. Jiajiin, and K. Kang, Phys. Rev. B **42**, 7450 (1990).
[61] T. Rajh, O. I. Mićić, and A. I. Nozik, J. Phys. Chem. **97**, 11999 (1993).
[62] *Semiconductors, Group IV Elements and III-V Compounds*, edited by O. Madelung (Springer-Verlag, Berlin, 1991).
[63] M. L. Cohen and J. R. Chelikowsky, *Electronic Structure and Optical Properties of Semiconductors* (Springer-Verlag, Berlin, 1989).
[64] L. Ley, R. A. Pollak, F. R. McFeely, S. P. Kowalczyk, and D. A. Shirley, Phys. Rev. B **9**, 600 (1974).
[65] D. E. Eastman, W. D. Grobman, J. L. Freeouf, and M. Erbudak, Phys. Rev. B **9**, 3473 (1974).
[66] D. E. Aspnes and A. A. Studna, Phys. Rev. B **7**, 4605 (1973).
[67] T. C. Chiang, J. A. Knapp, M. Aono, and D. E. Eastman, Phys. Rev. B **21**, 3513 (1980).
[68] O. I. Mićić, J. R. Sprague, C. J. Curtis, K. M. Jones, J. L. Machol, A. J. Nozik, H. Giessen, B. Fluegel, G. Mohs, and N. Peyghambrian, J. Phys. Chem. **99**, 7754 (1995).
[69] O. I. Mićić, C. J. Curtis, K. M. Jones, J. R. Sprague, and A. J. Nozik, J. Phys. Chem. **98**, 4966 (1994).
[70] N. W. Ashcroft and N. D. Mermin, *Solid State Physics* (Sanders, Fort Worth, 1976), p. 77.